Chemical Engineering Journal 492 (2024) 151682

Contents lists available at ScienceDirect

Chemical Engineering Journal

journal homepage: www.elsevier.com/locate/cej

Two-dimensional phthalocyanine-based molecular additives realize efficient hole transport and enhanced ion immobilization for durable perovskite solar cells

Zhihan Liao [a,1], Zekeriya Biyiklioglu [b,1], Li Yang [a,c,*], Hüseyin Baş [b], Peiyao Dong [a], Jianfei Hu [a], Jidong Deng [a], Xiaofeng Li [a], Yinhu Gao [a], Emre Güzel [d,*], Jinbao Zhang [a,c,*]

[a] College of Materials, Fujian Key Laboratory of Advanced Materials, Xiamen Key Laboratory of Electronic Ceramic Materials and Devices, Xiamen University, Xiamen 361005, China
[b] Karadeniz Technical University, Faculty of Science, Department of Chemistry, Trabzon, Turkiye
[c] Shenzhen Research Institute of Xiamen University, Shenzhen 518000, China
[d] Sakarya University of Applied Sciences, Faculty of Technology, Department of Engineering Fundamental Sciences, 54050 Sakarya, Turkiye

ARTICLE INFO

Keywords:
Phthalocyanine
Hole transport layer
Perovskite
Stability
Solar Cells

ABSTRACT

Perovskite solar cells (PSCs) have demonstrated high promises in low-cost manufacture and outstanding power conversion efficiencies (PCEs), however, long-term operational stability has become the major obstacle challenging the scalable application of this technology. Although the state-of-the-art hole transport layer (HTL) based on Spiro-OMeTAD becomes the indispensable component in high-efficiency PSCs, the dopants in the HTLs cause severe stability issues of ion migration and phase segregation, all of which induce the degradation of HTLs in the aspects of film conductivity and microstructures. Here we rationally design a two-dimensional phthalocyanine-based molecular additive (TB-C8-Ni) for the HTLs in order to enhance the carrier transportation and immobilize the ions. The incorporation of [8-(4-*tert*-butylphenoxy)octyl]oxy alkyl units as the side groups in TB-C8-Ni is essential to increase the solubility and improve the HTL uniformity. The superior planar structure of TB-C8-Ni favors the hole transportation and suppresses the migration of lithium ion under the environmental stress, which achieves reliable HTLs and devices. Consequently, the devices based on TB-C8-Ni exhibit boosted open-circuit voltage and fill factor, delivering an increased efficiency from 20.93% to 22.34%. More importantly, the additive TB-C8-Ni in the HTLs reinforces the moisture stability of devices, enabling to maintain 90% of initial efficiency after 2300 h in air.

1. Introduction

Faced with an energy crisis, the photovoltaic sector has attracted a lot of fascination, particularly with respect to thin-film perovskite solar cells (PSCs) that can convert light energy into electricity [1]. PSCs have ushered in a period of vigorous development, with power conversion efficiencies (PCEs) exceeding 26% [2]. The complete device structure of PSC is made up of several layers, including an absorbing layer that generates electrons and holes together with transport layers that collect charges. In the majority of devices with a n-i-p architecture, Spiro-OMeTAD acts as an indispensable component to transport the holes and achieves the record efficiencies [3,4]. In the actual application, high performance of Spiro-OMeTAD highly relies on the addition of dopants, such as lithium bis (trifluoromethanesulfonyl)imide (LiTFSI) and *tert*-butyl pyridine (tBP) in order to improve the electrical conductivity of the corresponding films [5]. However, recent studies have revealed that the hygroscopic nature of LiTFSI and the volatile properties of tBP cause severe morphological deformation and film degradation under the stress of heat or moisture, which hampers the long-term stability and future applications [5–7]. Although a variety of alternative dopants were developed for Spiro-OMeTAD, it remains a challenging issue to balance the efficiency and stability [8].

Planar macrocycle molecules, such as phthalocyanines, generally have outstanding optoelectronic properties and superior hydrophobicity

* Corresponding authors.
E-mail addresses: li.yang@xmu.edu.cn (L. Yang), eguzel@subu.edu.tr (E. Güzel), jinbao.zhang@xmu.edu.cn (J. Zhang).
[1] These authors contributed equally.

https://doi.org/10.1016/j.cej.2024.151682
Received 12 January 2024; Received in revised form 22 April 2024; Accepted 25 April 2024
Available online 9 May 2024

[9]. Besides, the phthalocyanines with long alkyl chains are soluble to organic solvents [10]. More importantly, these features can be well adjusted by displacing the central atom or altering the structure of the periphery [11]. Owing to high structural versatility of phthalocyanines, they have been serving as different functional materials in PSCs, such as hole transport layers (HTLs), additives in HTLs and interfacial layers on the perovskite layer [12]. Although the structural optimization of phthalocyanines-based HTLs triggers the advances of device stability, their PCEs still lag behind that of Spiro-OMeTAD-based devices. The low efficiencies are mostly resulted from the mismatch of the energy levels between the phthalocyanine-based materials and the perovskite, which leads to difficulties in carrier collection and induces severe carrier recombination at this interface [13]. Phthalocyanine molecules tend to aggregate in the film due to strong molecular stacking affinity, which would interrupt the hole transport, thus causing poor charge-transport performance [10,14]. Moreover, the poor interfacial contacts between phthalocyanine materials and the perovskite layers could inhibit the hole injection and collection, affecting the photovoltaic parameters in the devices [14].

In this work, we combine the advantages of phthalocyanines and Spiro-OMeTAD by developing hybrid HTLs. The designed molecule (TB-C8-Ni) contains four [8-(4-*tert*-butylphenoxy)octyl]oxy units at the peripheral position and a core of a metal atom. We find that the planar TB-C8-Ni could form better contact with Spiro-OMeTAD, which facilitates the hole transportation, leading to effective charge separation and migration. Besides, the two-dimensional molecules behave as a sheet-like barrier to mitigate the lithium-ion migration, improving the HTLs uniformity and device reliability. In addition, the HTLs with hydrophobic TB-C8-Ni protect the devices from the moisture infiltration and metal migration into the perovskite active layer. Consequently, the PSCs with the hybrid HTLs exhibit an improved efficiency of 22.34% compared to the control (20.93%). More encouragingly, the devices with TB-C8-Ni show impressive environmental stability by remaining 90% of the initial performance after 2300 h in air. This work provides an alternative strategy to enhance the charge transportation and film reliability of HTLs, and paves the way for further developing efficient and stable PSCs.

2. Results and discussion

The chemical structures of Spiro-OMeTAD and TB-C8-Ni are provided in Fig. 1a and b. The synthesis process, MALDI-TOF mass, nuclear magnetic resonance (NMR) spectroscopy (^{1}H NMR and ^{13}C NMR) and FT-IR spectra are presented in the supporting information (Scheme S1, Fig. S1-S8). The working mechanism of the TB-C8-Ni is displayed in Fig. 1**c.** To probe the effects of TB-C8-Ni in the HTLs, Fourier transform infrared (FTIR) spectroscopy of the corresponding films were measured (Fig. 2**a**). As for the hybrid HTLs with Spiro-OMeTAD and TB-C8-Ni, no additional peaks were observed from the FTIR spectra compared to the HTLs without TB-C8-Ni. This indicates little interaction between the Spiro-OMeTAD and TB-C8-Ni, which may be due to the small quantity of TB-C8-Ni [15]. Ultraviolet−visible (UV−vis) absorption spectra of the HTLs with TB-C8-Ni were carried out to further explore the impact of the TB-C8-Ni (Fig. 2**b**). Notably, the samples displayed an absorption peak at 675 nm which can be assigned to the signal from TB-C8-Ni [10], as shown in Fig. S9. At the peak position of 525 nm, negligible change was observed after the addition of TB-C8-Ni, meaning that the TB-C8-Ni does not involve in the oxidation process of Spiro-OMeTAD [16]. We also measured the water contact angle (θ) to test the water resistance of films before and after adding TB-C8-Ni (Fig. 2**c**). Surprisingly, the film with TB-C8-Ni (95.2°) exhibited much higher θ than the control film (79.8°), which could be mostly attributed to the long side chains in TB-C8-Ni [17]. The hydrophobic properties of the hybrid HTLs would increase the water-repellent ability and the HTL stability under the humid conditions.

According to the steady-state photoluminescence (PL) results (Fig. 2**d**), the device with TB-C8-Ni displayed lower PL intensity than the control, which suggests that more efficient charge injection in the films

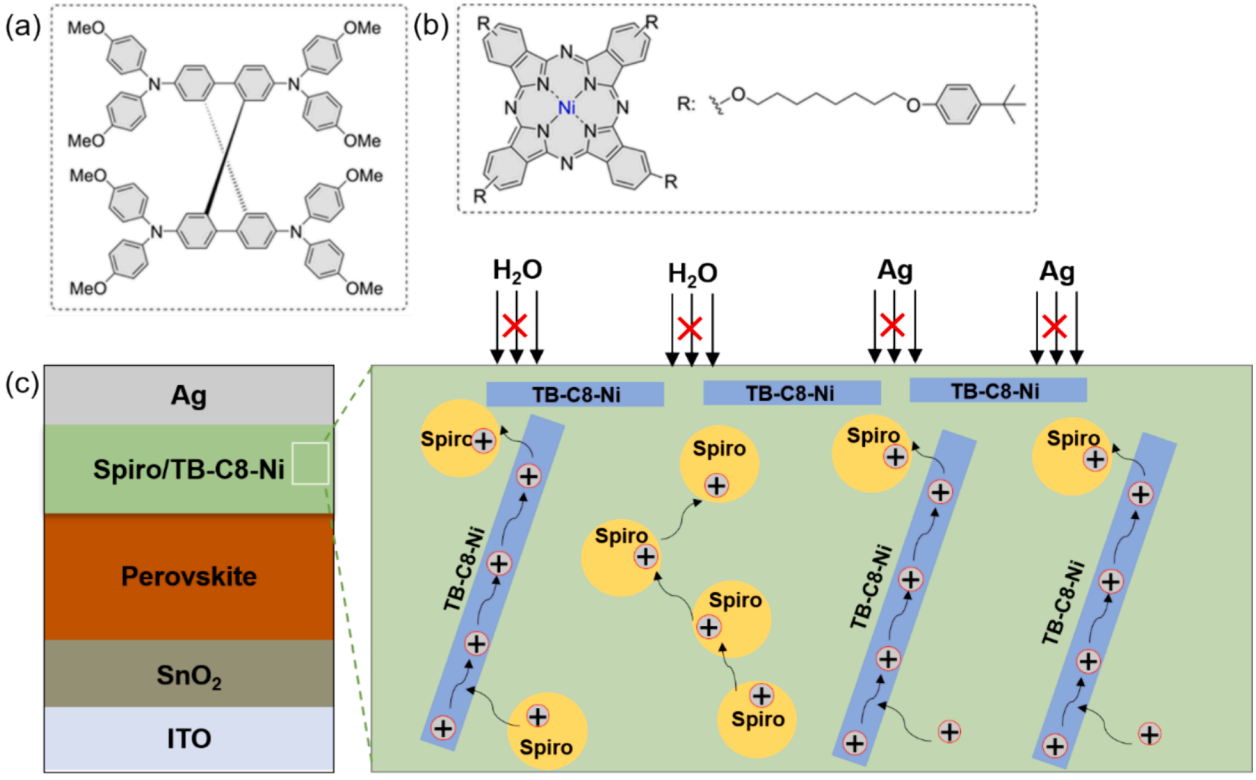

Fig. 1. (a) Molecular structure of Spiro-OMeTAD. (b) Molecular structure of TB-C8-Ni. (c) Schematic illustration of the as-prepared PSCs and the proposed working mechanism of hybrid HTLs with TB-C8-Ni.

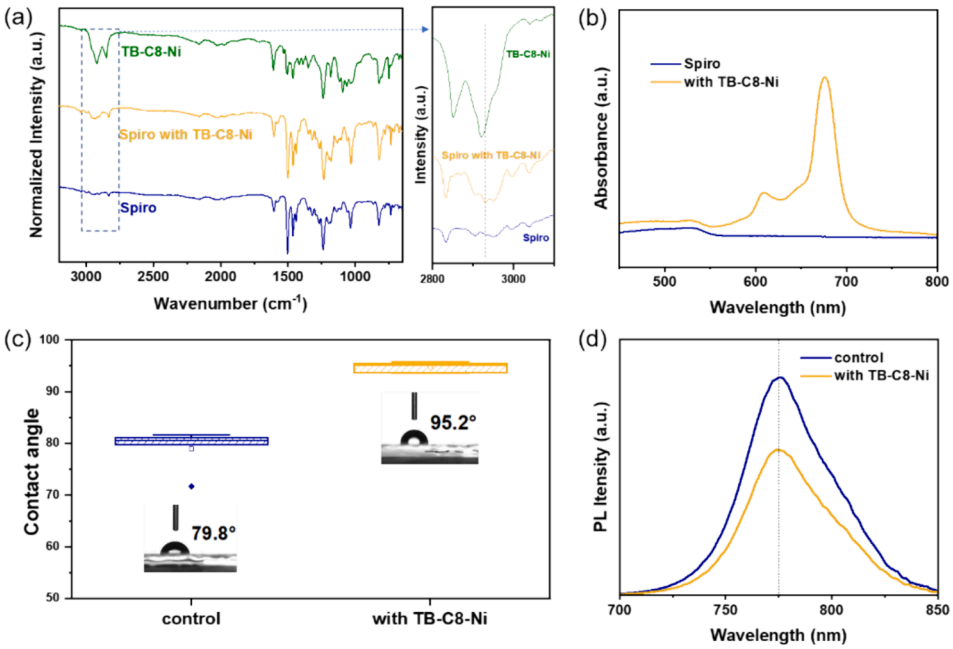

Fig. 2. (a) FTIR spectra of the films based on TB-C8-Ni, Spiro-OMeTAD and Spiro-OMeTAD with TB-C8-Ni (deposited on the glass). (b) UV–vis spectra of Spiro-OMeTAD and the mixture of Spiro-OMeTAD and TB-C8-Ni. (c) The water contact angles (θ) of different films, and (d) Steady-state photoluminescence spectra of the samples with the structure of HTL/perovskite/glass.

with TB-C8-Ni [18]. As shown in Fig. S10, the time-resolved PL (TRPL) results further proved the faster hole transfer process in the devices containing TB-C8-Ni by showing a shorter PL lifetime [19]. We also noticed that the PL mapping of the samples with TB-C8-Ni had a relatively lower intensity across the film (Fig. 3a and b), which is consistent with the observation in the PL results. The scanning electron microscopy (SEM) was used to study the impacts of TB-C8-Ni on the film morphology of the HTLs, and no obvious change in the film morphology was obtained from Fig. S11. As the concentration of TB-C8-Ni in the Spiro-OMeTAD increased, the HTLs underwent a significant morphology deformation with notable cracks in the films (Fig. S12). The atomic force microscopy (AFM) was employed to further explore the change of the film micromorphology (Fig. 3c and d). The roughness of the film was reduced after the incorporation of TB-C8-Ni by showing a root mean square (RMS) roughness of 2.853 nm compared to the control (5.494 nm), which was confirmed by the overall height distribution across the film (Fig. 3**h**). The high uniformity and smooth surface in the HTLs with TB-C8-Ni is critical for interfacial charge collection and interfacial stability (Fig. S11) [15]. In addition, it can be determined by the Kelvin probe force microscopy (KPFM) (Fig. 3**e–g**) that the TB-C8-Ni film exhibited a lower surface potential, which would be advantageous for interfacial hole transfer and the inhibition of carrier recombination [20].

In order to investigate the influence of TB-C8-Ni on the photovoltaic performance, the devices with a structure of ITO/SnO_2/$FA_{0.90}Cs_{0.07}MA_{0.03}PbI_{2.76}Br_{0.24}$/HTLs/Ag were fabricated, in which the HTLs were

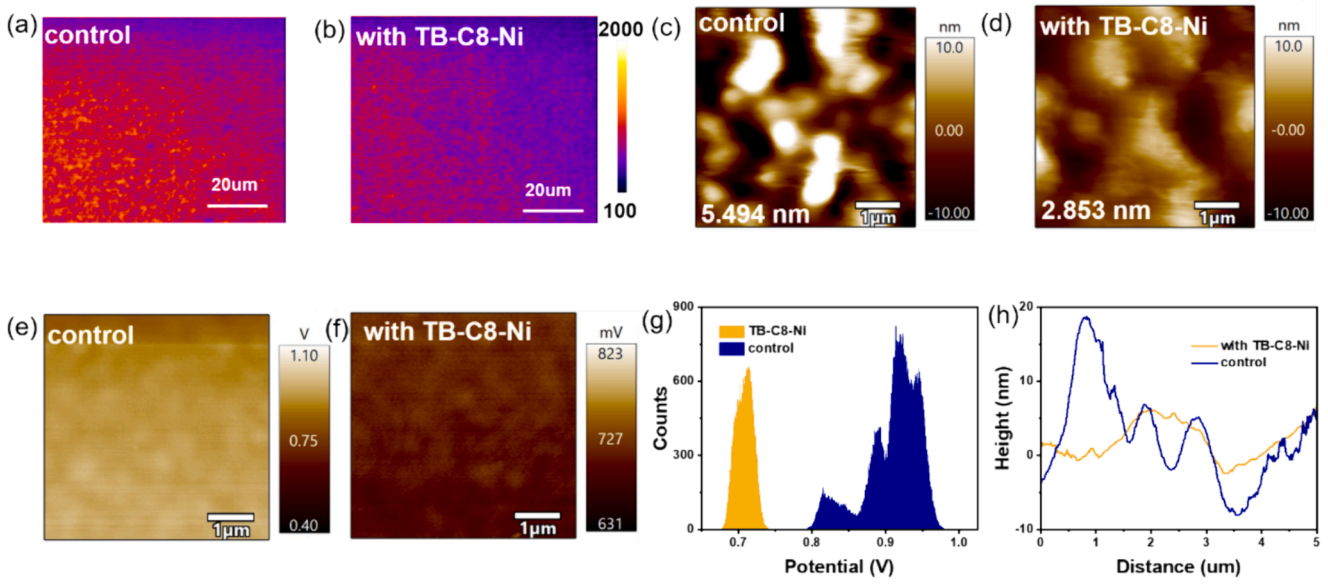

Fig. 3. (a) and (b) PL mapping, (c) and (d) AFM images, (e) and (f) KPFM images of films based on different HTLs. (g) The statistical distribution of surface potential from KPFM images in (e) and (f). (h) The line profiles of height from AFM images in (c) and (d).

based on hybrid composition of TB-C8-Ni with varying concentrations. The detailed photovoltaic parameters are presented in Fig. 4 **a-c** and Fig. S13. After the optimization, the device based on TB-C8-Ni (0.5 mg/mL) achieved the highest performance with a PCE of 22.34%, open-circuit voltage (V_{OC}) of 1.13 V, short-circuit current density (J_{SC}) of 24.12 mA/cm^2, and fill factor (*FF*) of 81.95%, as shown in Fig. 4**d**. All the parameters have been improved in the devices with hybrid HTLs compared to the control (PCE = 20.93%, V_{OC} = 1.10 V, J_{SC} = 24.22 mA/cm^2, *FF* = 78.47%). When the concentration was increased to 3 mg/mL, the V_{OC} of the devices was decreased (Fig. 4b), which could be attributed to higher charge recombination in the condition of excess TB-C8-Ni [13,21]. To better understand the charge dynamics, Mott-Schottky plots were used to estimate the built-in potential (V_{bi}) values of the PSCs (Fig. 4**e**). The V_{bi} was enhanced from 1.04 to 1.09 V after the addition of TB-C8-Ni, which would be favorable for the carrier separation and transportation [22]. We also examined the space charge limited current (SCLC) to evaluate the carrier mobility of the HTLs by using the structure of ITO/PEDOT:PSS/HTL/Ag (Fig. 4**f**) [23]. Encouragingly, the addition of TB-C8-Ni contributed to an improvement of carrier mobility, which was further proved by the conductivity measurement (Fig. 4**g**). In the hole-only device of ITO/HTL/Ag, the incorporation of TB-C8-Ni in the HTLs induced a decreased hole injection barrier and higher conductivity compared to the control [24,25]. The dark *J-V* measurement (Fig. 4**h**) implied that the TB-C8-Ni devices with a lower leakage current had reduced carrier losses at the interfaces [26]. Transient photovoltage (TPV) measurement was performed to verify the carrier recombination (Fig. 4**i**). The voltage attenuation with TB-C8-Ni was slower than the control, and the longer lifetime infers suppressed recombination under the support of TB-C8-Ni [27,28]. This effect could be further supported by electrochemical impedance spectra (EIS) (Fig. S14). These results demonstrate that TB-C8-Ni in the HTLs assists in the charge extraction and transportation, and simultaneously reduces the carrier losses, all of which are critical for realizing outstanding efficiencies in the devices.

To explore the effects of TB-C8-Ni on the HTL durability, we applied time-of-flight secondary ion mass spectroscopy (ToF-SIMS) to visualize the ion distribution in humid environment (70% RH). As shown in Fig. 5**a and 5b**, I^- in the perovskite layers obviously migrated into the HTLs in the control sample [29]. The 3D mapping of I_2^- further verified the phenomenon of I^- diffusion into HTLs. In contrast, I^- was remained in the perovskite films without notable migration into the HTLs containing TB-C8-Ni (Fig. 5**b**), suggesting that the iodine diffusion from the perovskite layers was effectively suppressed by the TB-C8-Ni [30]. To

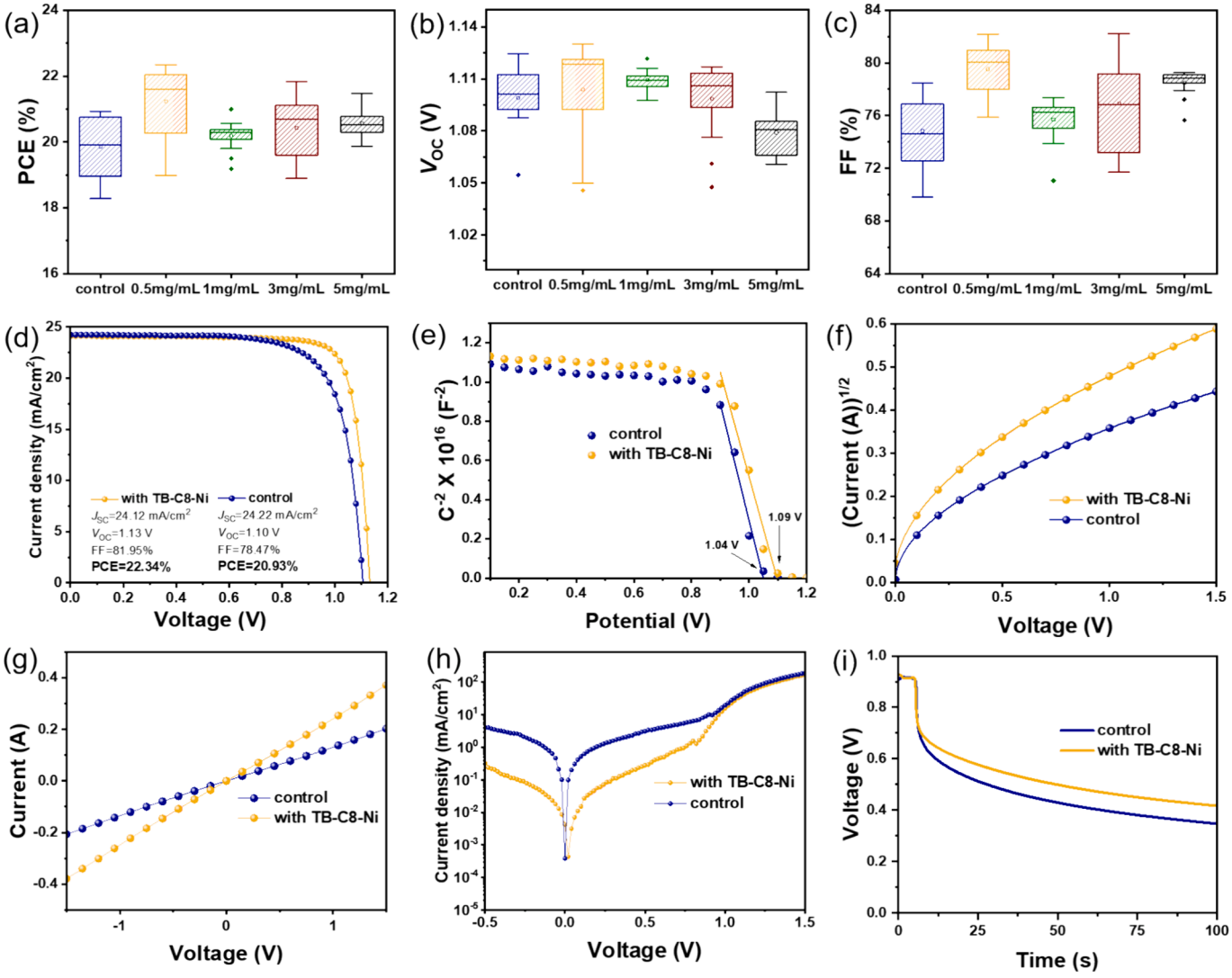

Fig. 4. (a), (b) and (c) Statistical photovoltaic parameters of the devices. (d) *J*−*V* curves of the champion devices. (e) Mott–Schottky measurement for the devices with or without TB-C8-Ni. (f) Space charge limited current (SCLC) curves of the devices with or without TB-C8-Ni (the architecture is ITO/PEDOT:PSS/HTL/Ag). (g) The conductivity curves of the devices with or without TB-C8-Ni (the architecture is ITO/HTL/Ag). (h) Dark J-V curves for the devices with or without TB-C8-Ni. (i) Transient photovoltage decay measurements of the devices with or without TB-C8-Ni.

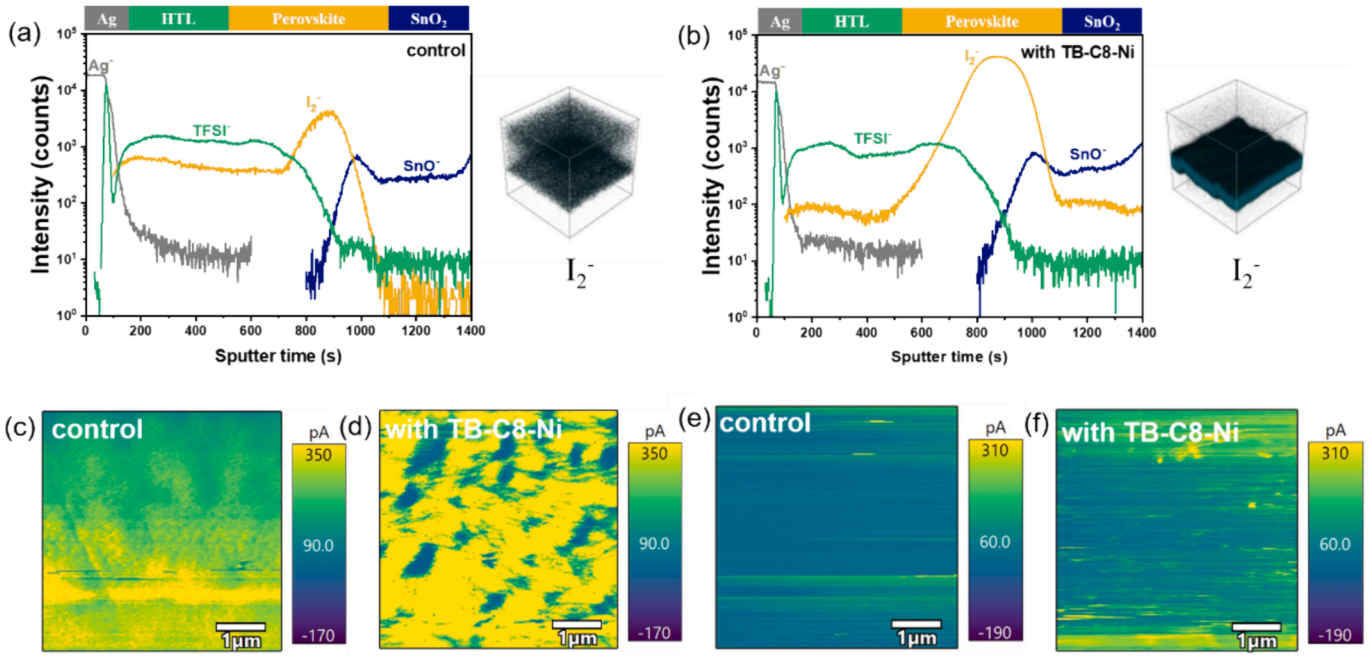

Fig. 5. (a) and (b) ToF-SIMS depth profiles and 3D I_2 mapping of the PSCs after storage in ambient air for 53 h (70% RH). (c) and (d) C-AFM images of HTL based on the perovskite films after storage in ambient air for 53 h (70% RH). (e) and (f) C-AFM images of HTL based on the perovskite films after heating at 85℃ for 9 h.

further investigate this effect, we examined the FTIR spectra of PbI_2, TB-C8-Ni, and their mixture, as shown in Fig. S15, and we observed the peak shift from 1617 cm^{-1} to 1621 cm^{-1}, which indicates an interaction between PbI_2 and the unsaturated atoms in the macrocyclic structure of TB-C8-Ni, as similarly reported in previous work [31,32]. Conductive atomic force microscope (C-AFM) was conducted to measure the electrical conductivity of the films under the humid and thermal stress (Fig. 5**c-5f**). Compared to the control, the HTLs with TB-C8-Ni showed higher spatial current and maintained much higher conductivity in the films under the humid condition, which could be a result of the high hydrophobicity of TB-C8-Ni [33].

We further measured the morphological change of the HTLs under the environment of high moisture and temperature by SEM. When subjected to a humid atmosphere (50–70% RH, 30℃), the hydrophilic salts (LiTFSI) appeared and gathered on the surface in the control films, causing severe morphological deformation (Fig. 6**a** and Fig. S16**a**) [34]. In the case of the film with TB-C8-Ni, the HTL morphology remained unchanged after 24 h (Fig. 6**b** and Fig. S16**b**). To explore whether TB-C8-Ni form interaction with lithium salts, we examined the FTIR spectra of LiTFSI, TB-C8-Ni, and their mixture. As shown in Fig. S17, the peak assigned to C−SO_2−H bond in LiTFSI was shifted from 1145 cm^{-1} to 1141 cm^{-1} after mixing with TB-C8-Ni [35]. In terms of TB-C8-Ni, the −CH_2− bond and the −CH_3 bond stemmed from the alkyl chains were shifted from 2857 cm^{-1} to 2849 cm^{-1} and from 2931 cm^{-1} to 2918 cm^{-1}. These results indicate that TB-C8-Ni could interact with LiTFSI, thus mitigating the aggregation of the lithium ions and HTL degradation under harsh conditions.

Furthermore, we also tested the devices stability under harsh environment (Fig. 6**e** and Fig. S18). The control suffered a plunge to 80% of the original PCE value under a humid condition. But the devices with TB-C8-Ni retained more than 90% of the primitive efficiency under the same condition, which could be ascribed to high hydrophobicity of the HTLs. Viewed from the glass side, the color of the control devices turned yellow after leaving them in ambient condition for 368 h (for 583 hours in Fig. S19). UV–vis spectra were further examined to investigate the change of the perovskite films for 7 days in humid environment (50–70% RH, 30℃). Fig. S20 summarized the absorption intensity of perovskite films covered by different HTLs under the same condition. The absorbance of the HTLs with TB-C8-Ni dropped more slowly compared to the control, which reckoned that the addition of TB-C8-Ni retarded the perovskite decomposition by protecting the perovskite layer from a damp circumstance.

We also tested the thermal stability of the devices by leaving the devices on a hot plate of 85℃ in the inert condition. The control underwent fast decomposition and damage after heating for 2 h, as displayed in Fig. 6**c** and Fig. S21**a**, which further reveals high vulnerability of the control HTLs to the heat. Encouragingly, the device with TB-C8-Ni remained intact morphology (Fig. 6**d** and Fig. S21**b**) under the same condition. TB-C8-Ni has a high thermal stability, which could enhance the film integrity and uniformity after thermal treatment. The evolution of the *J-V* curves further proved the improved stability of the devices with TB-C8-Ni (Fig. 6**f and 6 g**). The deterioration of the control device under the thermal condition may be due to the reaction between the migrated halide anions with the silver electrodes [36,37]. We further tested the long-term stability of the unsealed devices in the air storage (30℃, 30% RH), as depicted in Fig. 6**h** and Fig. S22. Notably, the introduction of TB-C8-Ni in the HTLs enhanced the device stability by maintaining 90% of the original PCEs after 2300 h, which emphasizes the critical roles of TB-C8-Ni in the improvement of device reliability.

3. Conclusion

The balance of efficiency and stability of Spiro-OMeTAD-based PSCs has become an important issue limiting the application of conventional PSCs. To enhance the reliability of the HTLs, an effective phthalocyanine-based molecular additive was designed and synthesized. The molecule tetra-[8-(4-*tert*-butylphenoxy)octyl]oxy substituted nickel(II) phthalocyanine (TB-C8-Ni) was incorporated with superior alkyl side groups and core metal ions, which contributed to high solubility and suppressed aggregation in the HTLs. As a result, the integration of TB-C8-Ni in the HTLs enabled significant improvement in the film properties and device performance. Specifically, the incorporation of TB-C8-Ni in the HTLs facilitated the carrier transportation and hole conductivity. Besides, the two-dimensional TB-C8-Ni could inhibit the iodide migration towards metal electrodes, which was essential for suppression of the device degradation. Based on the additive of TB-C8-

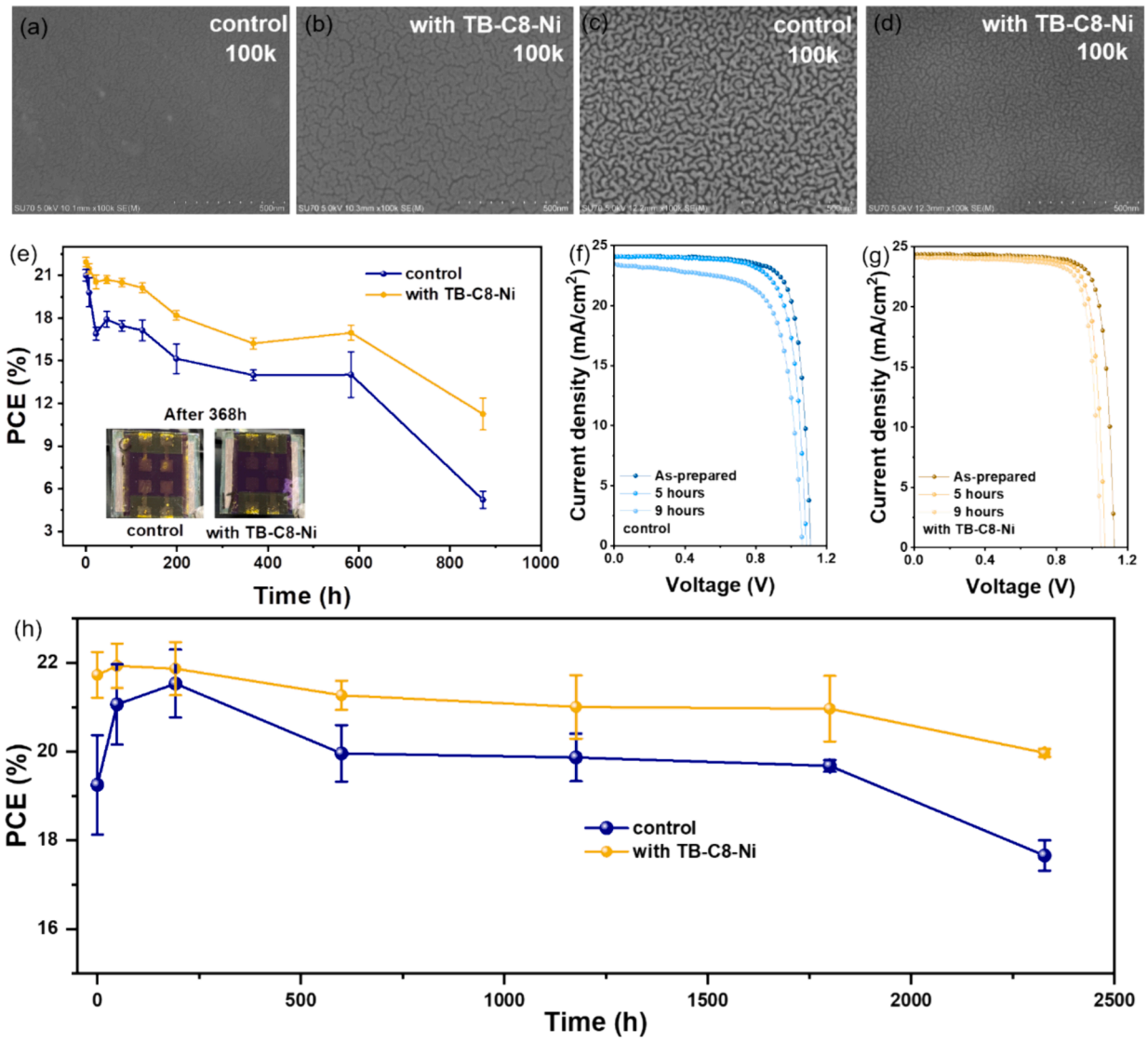

Fig. 6. (a) and (b) The SEM images of HTL (on perovskite layer) in the environment (30°C, 50–70% RH) for 24 h. (c) and (d) The SEM images of HTL (on perovskite layer) after heating 2 h at 85℃. (e) PCE evolution of the unencapsulated devices with or without TB-C8-Ni in the environment (30°C, 50–70% RH) for 872.5 h. (f) and (g) The *J*–*V* curves of as-prepared and after heating at 85°C. (h) PCE evolution of the unencapsulated devices with or without TB-Ni in a drying cabinet (30°C, 30% RH).

Ni, the devices achieved notable efficiency enhancement to 22.34% compared to the control (20.93%). More encouragingly, the TB-C8-Ni based devices showed superior stability in the humid environment by sustaining 91% of the initial PCEs for 124 h (50–70% RH), and 90% of original performance after 2300 h (30℃, 30% RH).

CRediT authorship contribution statement

Zhihan Liao: Writing – review & editing, Writing – original draft, Methodology, Investigation. **Zekeriya Biyiklioglu:** Writing – review & editing, Methodology, Investigation. **Li Yang:** Writing – review & editing, Writing – original draft, Methodology, Investigation. **Hüseyin Baş:** Writing – review & editing, Methodology, Investigation. **Peiyao Dong:** Methodology, Investigation. **Jianfei Hu:** Methodology, Investigation. **Jidong Deng:** Methodology, Investigation. **Xiaofeng Li:** Methodology, Investigation. **Yinhu Gao:** Methodology, Investigation. **Emre Güzel:** Writing – review & editing, Writing – original draft, Supervision, Methodology, Investigation. **Jinbao Zhang:** Writing – review & editing, Writing – original draft, Project administration, Methodology, Investigation.

Declaration of competing interest

The authors declare that they have no known competing financial interests or personal relationships that could have appeared to influence the work reported in this paper.

Data availability

Data will be made available on request.

Acknowledgments

This work was financially supported by National Natural Science Foundation of China (52102309, 22379126, 22309154), Guangdong Basic and Applied Basic Research Foundation (2022A1515011869), Shenzhen Science and Technology Program (JCYJ20220530143201004, JCYJ20220530143214032), Fundamental Research Funds for the Central Universities (20720220107), Natural Science Foundation of Fujian Province of China (2021 J01040), Nanqiang Youth Talented Program of Xiamen University, Scientific Research

Projects Coordination Unit of Sakarya University of Applied Sciences (212-2024). The authors thank the Tan Kah Kee Innovation Laboratory (IKKEM) of Xiamen University for the assistance on measurements.

Appendix A. Supplementary data

Supplementary data to this article can be found online at https://doi.org/10.1016/j.cej.2024.151682.

References

[1] A.S. Bati, Y.L. Zhong, P.L. Burn, M.K. Nazeeruddin, P.E. Shaw, M. Batmunkh, Next-generation applications for integrated perovskite solar cells, Commun. Mater. 4 (2023) 2.
[2] H. Zhu, S. Teale, M.N. Lintangpradipto, S. Mahesh, B. Chen, M.D. McGehee, E. H. Sargent, O.M. Bakr, Long-term operating stability in perovskite photovoltaics, Nat. Rev. Mater. 8 (2023) 569–586.
[3] J.Y. Seo, S. Akin, M. Zalibera, M.A.R. Preciado, H.S. Kim, S.M. Zakeeruddin, J. V. Milić, M. Grätzel, Dopant engineering for SPIRO-OMeTAD hole-transporting materials towards efficient perovskite solar cells, Adv. Funct. Mater. 31 (2021) 2102124.
[4] G. Du, L. Yang, C. Zhang, X. Zhang, N. Rolston, Z. Luo, J. Zhang, Evaporated undoped spiro-OMeTAD enables stable perovskite solar cells exceeding 20% efficiency, Adv. Energy Mater. 12 (2022) 2103966.
[5] X. Liu, B. Zheng, L. Shi, S. Zhou, J. Xu, Z. Liu, J.S. Yun, E. Choi, M. Zhang, Y. Lv, W.-H. Zhang, J. Huang, C. Li, K. Sun, J. Seidel, M. He, J. Peng, X. Hao, M. Green, Perovskite solar cells based on spiro-OMeTAD stabilized with an alkylthiol additive, Nat. Photonics 17 (2023) 96–105.
[6] C. Zhang, K. Wei, J. Hu, X. Cai, G. Du, J. Deng, Z. Luo, X. Zhang, Y. Wang, L. Yang, A review on organic hole transport materials for perovskite solar cells: Structure, composition and reliability, Mater. Today 67 (2023) 518–547.
[7] S. Liu, V.P. Biju, Y. Qi, W. Chen, Z. Liu, Recent progress in the development of high-efficiency inverted perovskite solar cells, NPG Asia Mater. 15 (2023) 27.
[8] G. Ren, W. Han, Y. Deng, W. Wu, Z. Li, J. Guo, H. Bao, C. Liu, W. Guo, Strategies of modifying spiro-OMeTAD materials for perovskite solar cells: a review, J. Mater. Chem. A 9 (2021) 4589–4625.
[9] D. Molina, J. Follana-Berná, Á. Sastre-Santos, Phthalocyanines, porphyrins and other porphyrinoids as components of perovskite solar cells, J. Mater. Chem. C 11 (2023) 7885–7919.
[10] E. Rezaee, D. Khan, S. Cai, L. Dong, H. Xiao, S.R.P. Silva, X. Liu, Z.-X. Xu, Phthalocyanine in perovskite solar cells: a review, Mater. Chem Front. 7 (2023) 1704–1736.
[11] M. Urbani, G. de la Torre, M.K. Nazeeruddin, T. Torres, Phthalocyanines and porphyrinoid analogues as hole-and electron-transporting materials for perovskite solar cells, Chem. Soc. Rev. 48 (2019) 2738–2766.
[12] Y. Matsuo, K. Ogumi, I. Jeon, H. Wang, T. Nakagawa, Recent progress in porphyrin-and phthalocyanine-containing perovskite solar cells, RSC Adv. 10 (2020) 32678–32689.
[13] H. Kim, K.S. Lee, M.J. Paik, D.Y. Lee, S.U. Lee, E. Choi, J.S. Yun, S.I. Seok, Polymethyl methacrylate as an interlayer between the halide perovskite and copper phthalocyanine layers for stable and efficient perovskite solar cells, Adv. Funct. Mater. 32 (2022) 2110473.
[14] Y. Kim, T.-Y. Yang, N. Jeon, J. Im, S. Jang, T. Shin, H.-W. Shin, S. Kim, E. Lee, J. Noh, Engineering interface structures between lead halide perovskite and copper phthalocyanine for efficient and stable perovskite solar cells, Energy Environ. Sci. 10 (2017) 2109–2116.
[15] H. Yang, Y. Shen, R. Zhang, Y. Wu, W. Chen, F. Yang, Q. Cheng, H. Chen, X. Ou, H. Yang, Composition-conditioning agent for doped spiro-OMeTAD to realize highly efficient and stable perovskite solar cells, Adv. Energy Mater. 12 (2022) 2202207.
[16] X. Li, W. Wang, K. Wei, J. Deng, P. Huang, P. Dong, X. Cai, L. Yang, W. Tang, J. Zhang, Conjugated phosphonic acids enable robust hole transport layers for efficient and intrinsically stable perovskite solar cells, Adv. Mater. 36 (2024) 2308969.
[17] C. Chen, H. Li, J. Jin, Y. Cheng, D. Liu, H. Song, Q. Dai, Highly enhanced long time stability of perovskite solar cells by involving a hydrophobic hole modification layer, Nano Energy 32 (2017) 165–173.
[18] J. Zheng, Z. Ying, Z. Yang, Z. Lin, H. Wei, L. Chen, X. Yang, Y. Zeng, X. Li, J. Ye, Polycrystalline silicon tunnelling recombination layers for high-efficiency perovskite/tunnel oxide passivating contact tandem solar cells, Nat. Energy 8 (2023) 1250–1261.
[19] C. Liu, R. Lin, Y. Wang, H. Gao, P. Wu, H. Luo, X. Zheng, B. Tang, Z. Huang, H. Sun, Efficient All-Perovskite Tandem Solar Cells with Low-Optical-Loss Carbazolyl Interconnecting Layers, Angew. Chem., Int. Ed. 62 (2023) e202313374.
[20] H. Zhu, B. Shao, J. Yin, Z. Shen, L. Wang, R.W. Huang, B. Chen, N. Wehbe, T. Ahmad, M. Abulikemu, Retarding Ion Migration for Stable Blade-Coated Inverted Perovskite Solar Cells, Adv. Mater. 36 (2023) 2306466.
[21] J. Seo, N.J. Jeon, W.S. Yang, H.W. Shin, T.K. Ahn, J. Lee, J.H. Noh, S.I. Seok, Effective electron blocking of CuPC-doped spiro-OMeTAD for highly efficient inorganic-organic hybrid perovskite solar cells, Adv. Energy Mater. 5 (2015) 1501320.
[22] L. Qi, G. Du, G. Zhu, Y. Wang, L. Yang, J. Zhang, Enhanced interface compatibility by ionic dendritic molecules to achieve efficient and stable perovskite solar cells, ACS Appl. Mater. Interfaces 15 (2023) 41109–41120.
[23] P. Dong, L. Yang, G. Du, W. Wang, N. Rolston, J. Zhang, Anion-modulated chemical doping of organic hole conductor boosts efficiency and stability of perovskite solar cells, Adv. Funct. Mater. 33 (2023) 2211304.
[24] H. Zai, J. Su, C. Zhu, Y. Chen, Y. Ma, P. Zhang, S. Ma, X. Zhang, H. Xie, R. Fan, Sandwiched electrode buffer for efficient and stable perovskite solar cells with dual back surface fields, Joule 5 (2021) 2148–2163.
[25] H. Yang, R. Li, S. Gong, H. Wang, S.M. Qaid, Q. Zhou, W. Cai, X. Chen, J. Chen, Z. Zang, Multidentate chelation achieves bilateral passivation toward efficient and stable perovskite solar cells with minimized energy losses, Nano Lett. 23 (2023) 8610–8619.
[26] D. Xu, Z. Gong, Y. Jiang, Y. Feng, Z. Wang, X. Gao, X. Lu, G. Zhou, J.-M. Liu, J. Gao, Constructing molecular bridge for high-efficiency and stable perovskite solar cells based on P3HT, Nat. Commun. 13 (2022) 7020.
[27] C. Tian, Z. Zhang, A. Sun, J. Liang, Y. Zheng, X. Wu, Y. Liu, C. Tang, C.-C. Chen, Tuning phase stability and interfacial dipole for efficient methylammonium-free Sn-Pb perovskite solar cells, Nano Energy 116 (2023) 108848.
[28] Y. Wang, M. Feng, H. Chen, M. Ren, H. Wang, Y. Miao, Y. Chen, Y. Zhao, Highly crystalized Cl-doped SnO_2 nanocrystals for stable aqueous dispersion toward high-performance perovskite photovoltaics, Adv. Mater. 36 (2024) 2305849.
[29] J. Zhou, Z. Liu, P. Yu, G. Tong, R. Chen, L.K. Ono, R. Chen, H. Wang, F. Ren, S. Liu, J. Wang, Z. Lan, Y. Qi, W. Chen, Modulation of perovskite degradation with multiple-barrier for light-heat stable perovskite solar cells, Nat. Commun. 14 (2023) 6120.
[30] F. Cheng, S. Zhan, Y. Cai, F. Cao, X. Dai, R. Xu, J. Yin, J. Li, N. Zheng, B. Wu, Interfacial property tuning enables copper electrodes in high-performance n–i–p perovskite solar cells, J. Am. Chem. Soc. 145 (2023) 20081–20087.
[31] K. Zou, Q. Li, J. Fan, H. Tang, L. Chen, S. Tao, T. Xu, W. Huang, Pyridine derivatives' surface passivation enables efficient and stable carbon-based perovskite solar cells, ACS Mater. Lett. 4 (2022) 1101–1111.
[32] Q. Hu, E. Rezaee, W. Xu, R. Ramachandran, Q. Chen, H. Xu, T. El-Assaad, D. V. McGrath, Z.X. Xu, Dual defect-passivation using phthalocyanine for enhanced efficiency and stability of perovskite solar cells, Small 17 (2021) 2005216.
[33] X. Jiang, D. Wang, Z. Yu, W. Ma, H.B. Li, X. Yang, F. Liu, A. Hagfeldt, L. Sun, Molecular engineering of copper phthalocyanines: a strategy in developing dopant-free hole-transporting materials for efficient and ambient-stable perovskite solar cells, Adv. Energy Mater. 9 (2019) 1803287.
[34] X. Liu, B. Zheng, L. Shi, S. Zhou, J. Xu, Z. Liu, J.S. Yun, E. Choi, M. Zhang, Y. Lv, Perovskite solar cells based on spiro-OMeTAD stabilized with an alkylthiol additive, Nat. Photonics 17 (2023) 96–105.
[35] A. Wu, F. Lu, P. Sun, X. Qiao, X. Gao, L. Zheng, Low-molecular-weight supramolecular ionogel based on host–guest interaction, Langmuir 33 (2017) 13982–13989.
[36] A.K. Jena, M. Ikegami, T. Miyasaka, Severe morphological deformation of spiro-OMeTAD in (CH_3NH_3) PbI_3 solar cells at high temperature, ACS Energy Lett. 2 (2017) 1760–1761.
[37] Q. Lou, G. Lou, H. Guo, T. Sun, C. Wang, G. Chai, X. Chen, G. Yang, Y. Guo, H. Zhou, Enhanced efficiency and stability of n-i-p perovskite solar cells by incorporation of fluorinated graphene in the spiro-OMeTAD hole transport layer, Adv. Energy Mater. 12 (2022) 2201344.